

Near-Earth Asteroid 2005 CR37: Radar Images of a Candidate Contact Binary

Lance A. M. Benner^a, Michael C. Nolan^b, Steven J. Ostro^a, Jon D. Giorgini^a,
Christopher Magri^c, and Jean-Luc Margot^d

^aJet Propulsion Laboratory, California Institute of Technology, 4800 Oak Grove Drive, Pasadena, CA
91109, USA

^bNational Astronomy and Ionosphere Center, Arecibo Observatory, HC3 Box 53995, Arecibo, PR
00612, USA

^cUniversity of Maine at Farmington, 39 High Street, Preble Hall, Farmington, ME 04938, USA

^dDepartment of Astronomy, Cornell University, Ithaca, NY 14853, USA

24 manuscript pages

3 figures

4 tables

Proposed running head: Radar images of asteroid 2005 CR37

Address correspondence to:

Dr. Lance A. M. Benner

MS 300-233

Jet Propulsion Laboratory

California Institute of Technology

4800 Oak Grove Drive

Pasadena, CA 91109-8099

USA

Phone: 818-354-7412

Fax: 818-354-9476

Lance.Benner@jpl.nasa.gov

ABSTRACT

Arecibo (2380 MHz, 13 cm) radar observations of 2005 CR37 provide detailed images of a candidate contact binary: a 1.6-km-long, extremely bifurcated object. Although the asteroid's two lobes are round, there are regions of modest topographic relief, such as an elevated, 200-m-wide facet, that suggest that the lobes are geologically more complex than either coherent fragments or homogeneous rubble piles. Since January 1999, about 9% of NEAs larger than ~200 m imaged by radar have been candidate contact binaries.

Key words: asteroids; radar; surfaces, asteroids; asteroids, composition

OBSERVATIONS AND ORBIT REFINEMENT

2005 CR37 was discovered by H. Mikuz at Crni Vrh Observatory (Slovenia) on February 8, 2005 (M.P.E.C. 2005-C32, <http://cfa-www.harvard.edu/iau/mpec/K05/K05C32.html>). It immediately became clear that the object would make a close approach to Earth and, given its estimated absolute magnitude $H = 18.9$, would be a very strong radar target.

We observed it at Arecibo during a 2.3-hour interval on Feb. 23. We started with five "Doppler-only," continuous wave (CW) transmit-receive cycles (runs), measured a correction to the ephemeris, updated it, and did another CW run with the new ephemeris to verify the accuracy of its Doppler prediction. We then used setups with a time-delay resolution of 4 μs (600 meters) to measure the asteroid's range and concluded with 38 0.1- μs (15-m) imaging runs (Table 1).

Prior to radar detection, the 3σ uncertainties on 2005 Feb 26.0 were 180 Hz and 0.33 s (49,000 km). We used the coarse-resolution 4- μs ranging and high-resolution 0.1- μs imaging data to estimate two range corrections to the ephemeris. The single Doppler and two ranges give *a posteriori* 3σ Doppler and range uncertainties of 3.3 Hz and 255 μs (38 km), reductions by factors of ~ 54 in Doppler frequency and ~ 1300 in time delay.

The interval over which the pre-radar orbit could be integrated reliably (defined by when the 3σ uncertainty in the time of Earth close-approach is $\leq \pm 10$ days, or the 3σ uncertainty in Earth close-approach distance at the nominal time of the encounter is $\leq \pm 0.1$ AU, whichever occurs first) was

limited to 2005. Including the radar astrometry in a new orbit solution #30 (which includes 196 optical observations over 62 days along with the three radar measurements), the reliable close-approach prediction interval is extended to span 1784-3625, or about 1840 years (Table 2). Over that interval, the probability of Earth impact is effectively zero.

SHAPE, DIMENSIONS, AND SURFACE FEATURES

Our image sequence (Fig. 1) reveals an elongated and bifurcated shape with lobes that are round, have comparable dimensions, and are separated by a pronounced "neck." The images span about one-fourth of a rotation in an interval of 96 minutes, implying a rotation period of roughly 6 h. A photometrically-derived rotation period of 5.6 h was determined by D. Pray (pers. comm.) shortly after the radar observations concluded.

The echo bandwidth in the delay-Doppler images varies from 5.8 Hz end-on to 7.9 Hz broadside. However, noting that the orientation was closer to end-on at the start of the observations, we estimated the bandwidths from CW spectra processed to 0.1 Hz resolution and found that the minimum, 4.2 Hz, occurred during the first CW run. This places a lower bound on the elongation of $7.9/4.2 = 1.9$ and establishes that 2005 CR37 is a very elongated object, consistent with the 1.1-mag amplitude of Pray's lightcurve.

2005 CR37's elongation, in the top one-third among those reported from radar observations (http://echo.jpl.nasa.gov/~lance/nea_elongations.html), is comparable to the elongations of 2063 Bacchus (Benner et al. 1999b) and 25143 Itokawa (Ostro et al. 2004, 2005).

The first and last images in Fig. 1 have visible range extents of 1.1 km that establish a lower bound on the asteroid's longest dimension. The maximum bandwidth of 7.9 Hz and the 5.6 h rotation period

constrain the lower bound on the maximum pole-on dimension, D_{\max} , to be > 1.6 km. When the asteroid is oriented broadside, the visible range extent of each lobe is about 0.4 km. If the true range extents are about twice the visible range extents, as would be true for a sphere, then each lobe is about 0.8 km deep in this orientation.

The images suggest that the asteroid's 2-D pole-on silhouette has extreme bandwidths that are close to 1.6×0.8 km. If we pretend that its 3-D convex envelope is shaped like a biaxial ellipsoid, then its effective diameter (the diameter of a sphere with the same volume) is about 1 km. The actual effective diameter may be different due to concavities in the shape and the fact that the long axis may be longer than 1.6 km.

When oriented broadside, a valley with a depth of ~ 150 m is visible between the lobes. The neck also has a visible range extent of about 150; if it's symmetric with respect to the asteroid's long axis, then its true extent would be about 300 m.

Let us denote the left and right lobes in the images as Alpha and Beta. Figure 2 shows a collage of three enlarged images. Images obtained over a range of rotation phases show that the edge of Alpha adjacent to the neck appears angular, suggesting the presence of at least one facet. The facet is slightly raised away from the surface (Fig. 2A). Portions of Beta also appear to be faceted in images when Beta was closer to Earth than Alpha (Fig. 2C).

Other irregularities are present along the leading edge. In multiple images, a "hill" consisting of several pixels in delay is evident in the middle of Alpha's leading edge (Fig. 2B, 2C). The sequence in Fig. 2 suggests that the "hill" may be one end of the "raised facet" described above. Near the "neck," another feature visible in multiple images shows a curve of moderately bright pixels that partially bound an inner radar-dark region (Fig. 2B). A similar feature is evident in several images of Beta's leading

edge (Fig. 2C). These features give the impression of obliquely-viewed concavities, perhaps craters, and are similar to features seen on 53319 1999 JM8 (Benner et al. 2002).

A number of images also show a cluster of diffuse pixels located about 150 m behind Alpha's leading edge (arrow in Figs. 2A and 2C). They are faint in many frames but are more conspicuous when the images are shown as an animation (http://echo.jpl.nasa.gov/~lance/2005CR37/cr37_movie.mov). We interpret this feature as a modest topographic high that is barely visible due to the observing geometry. Another cluster of faint pixels appears on Beta in the last several frames and may also represent a positive relief feature.

DISC-INTEGRATED RADAR AND OPTICAL PROPERTIES

Radar cross sections estimated from each CW spectrum are listed in Table 3. The cross sections show a steady increase as a function of time, a pattern that matches the progression of increasing surface area oriented toward the radar in the images obtained shortly after the CW observations. This partial radar "lightcurve" is reminiscent of those obtained from 433 Eros (Jurgens and Goldstein 1976), 1685 Toro (Ostro et al. 1983), 1620 Geographos (Ostro et al. 1996), and 7822 1991 CS (Benner et al. 1999a).

The radar cross section from the sixth run was obtained when the asteroid was oriented close to midway between end-on and broadside. As such, it represents a first-order estimate of the average cross section, so let us adopt it as our nominal value and explore its implications.

If we adopt an effective diameter of 1 km, then a radar cross section of 0.19 km^2 yields a relatively bright radar albedo of 0.24 that is comparable to those obtained from several other NEAs. The radar

brightness could be explained by a low near-surface porosity (i.e. relatively near-surface density; Magri et al. 2001).

The circular polarization ratios of the spectra have a mean and rms dispersion of 0.32 ± 0.03 , which is indistinguishable from the average observed from other radar-detected NEAs. This indicates that the near-surface is moderately complex at decimeter scales (Ostro et al. 2002). Strong OC-only glints in runs 3, 4, and 6 may partly explain the dispersion in SC/OC (Fig. 3). Glints are also visible on the leading edge in several delay-Doppler images when the contrast has been stretched appropriately; when taken as a whole, the glints are consistent with the presence of facets that are evident in the delay-Doppler images, since large facets that are smooth at decimeter scales produce quasi-specular OC-only radar reflections.

DISCUSSION

Facets spanning lengths from tens of meters to more than 1 km are evident in radar images of 1620 Geographos (Ostro et al. 1996), 4179 Toutatis (Ostro et al. 1995), 6489 Golevka (Hudson et al. 2000), 53319 1999 JM8 (Benner et al. 2002), 54509 2000 PH5 (Taylor et al. 2004), and 11066 Sigurd (Benner et al. 2004), but the raised facet is unlike any seen in radar images other asteroids.

2005 CR37 clearly is bifurcated, but since our rotation-phase coverage is limited (and certainly insufficient for 3-D shape reconstruction), we don't know if the concavity between Alpha and Beta is a waist that encircles the long axis, in which case we should arguably describe the asteroid as having a "contact binary shape," or just a "dent" fortuitously seen in our images. Hence we designate 2005 CR37

as a candidate for being a true contact binary, i.e., an asteroid consisting of two lobes that are bound by gravity rather than tensile strength and that presumably once were separate.

Table 4 shows estimates of the dimensions and rotation periods of candidate contact binary NEAs imaged by radar: 4769 Castalia (Ostro et al. 1990; Hudson and Ostro 1994), 2063 Bacchus (Benner et al. 1999b), 4486 Mithra (Ostro et al. 2000), 11066 Sigurd (Benner et al. 2004), 2002 NY40 (Pravec et al. 2005), and several asteroids that have not been published. Although 4179 Toutatis is sometimes referred to as a contact binary, its mass distribution is not bimodal (Hudson and Ostro 1995, Hudson et al. 2003), so we do not consider it a candidate contact binary. 2005 CR37 has dimensions that are comparable to those of Castalia, 2001 KZ66, and perhaps 1993 OM7 and its rotation period is third fastest among those listed in the table.

Scheeres et al. (2004) have shown that the spin states of elongated NEAs can become slower and can change to non-principal axis (NPA) rotation due to tidal interactions during close encounters with Earth and Venus. The implication is that a rapidly rotating object such as 2005 CR37 may be relatively young while a slowly rotating, NPA rotator such as Mithra may be relatively old. In other words, elongated objects that rotate rapidly may not have had sufficient time for many close flybys that would alter their spin and place them into NPA rotation states.

The images of 2005 CR37 were obtained at a resolution equal to or higher than those of other candidate contact binaries, and they reveal an object with more surface structure than is evident on the other objects. The only other candidate contact binary imaged at comparable range and Doppler resolutions is 2002 NY40.

How did the structural complexity on 2005 CR37 originate? Leading mechanisms to form contact binaries are low-velocity collisions (Farinella 1992, Hudson and Ostro 1995, Chauvineau et al. 1995, Bottke and Melosh 1996a,b, Leinhardt et al. 2000), perhaps between components of true binaries, and

spin-up and shape distortion via tidal encounters with Earth and Venus (Asphaug and Benz 1996, Richardson et al. 1998) or due to asymmetric solar absorption and re-emission (Bottke et al. 2002). Other explanations, such as a sequence of impacts that sculpted the object into its present shape or an origin as an impact shard from catastrophic disruption of a larger progenitor, seem relatively contrived. For a contact binary formed by a low-velocity collision, morphologically complex terrain near the intersection of the lobes, as is seen on 2005 CR37, may be almost inevitable. This may explain the raised facet, which we speculate could be a fault block formed by compressional stresses during an impact.

The complex surface morphology on 2005 CR37 is somewhat more rugged than the generally smooth shapes produced by simulations of collisions or tidal distortion of agglomerates of gravitationally-bound spheres (Richardson et al 1998, Leinhardt et al. 2000). The raised facet hints that 2005 CR37 might be at least partially fractured and hence not monolithic. Perhaps its internal structure consists of an assemblage of irregularly-shaped blocks that span a distribution of sizes. Simulations of collisions or tidal distortion by such assemblages may clarify the various possibilities.

How abundant are contact binaries in the NEA population? Since January 1999 about 9% of NEAs larger than ~200 m imaged by radar have bifurcated shapes and can be considered candidate contact binaries (two possible contact binaries were imaged by radar prior to 1999: 4769 Castalia and 2063 Bacchus). The abundance of true binaries above the same size threshold imaged by radar during the same interval is about 17% (Margot et al. 2002, Merline et al. 2002, Pravec et al. 2005). If contact binaries and true binaries form by the same mechanisms, which has been suggested theoretically, then both types of objects should exist. Is there really a two-fold difference in the abundance of binaries and contact binaries in the NEA population? If so, then how can it be explained?

ACKNOWLEDGMENTS

We thank Riccardo Giovanelli for graciously relinquishing time at Arecibo on short notice so that we could observe 2005 CR37. We thank the technical staff at Arecibo for help with the observations. C. Magri is partially supported by NSF grant AST-0205974. Part of this research was conducted at the Jet Propulsion Laboratory, California Institute of Technology, under contract with the National Aeronautics and Space Administration (NASA). The Arecibo Observatory is part of the National Astronomy and Ionosphere Center, which is operated by Cornell University under a cooperative agreement with the National Science Foundation.

REFERENCES

- Asphaug, E., and Benz, W., 1996. Size, density, and structure of comet Shoemaker-Levy 9 inferred from the physics of tidal breakup. *Icarus* 121, 225-248.
- Benner, L.A.M., Ostro, S.J., Rosema, K.D., Giorgini, J.D., Choate, D., Jurgens, R.F., Rose, R., Slade, M.A., Thomas, M.L., Winkler, R., and Yeomans, D. K., 1999a. Radar observations of asteroid 7822 (1991 CS). *Icarus* 137, 247-259.
- Benner, L.A.M., Hudson, R.S., Ostro, S.J., Rosema, K.D., Giorgini, J.D., Yeomans, D.K., Jurgens, R.F., Mitchell, D.L., Winkler, R., Rose, R., Slade, M.A., and Thomas, M.L., 1999b. Radar observations of asteroid 2063 Bacchus. *Icarus* 139, 309-327.
- Benner, L.A.M., Ostro, S.J., Nolan, M.C., Margot, J.L., Giorgini, J.D., Hudson, R.S., Jurgens, R.F., Slade, M.A., Howell, E.S., Campbell, D.B., and Yeomans, D.K., 2002. Radar observations of asteroid 1999 JM8. *Meteorit. Planet. Sci.* 37, 779-792.
- Benner, L.A.M., Nolan, M.C., Carter, L.M., Ostro, S.J., Giorgini, J.D., Magri, C., and Margot, J.L., 2004. Radar imaging of near-Earth asteroid 11066 Sigurd. *Bull. Am. Astron. Soc.* 36, #32.29.
[Abstract]
- Bottke, W.F., and Melosh, H.J., 1996a. Formation of asteroid satellites and doublet craters by planetary tidal forces. *Nature* 381, 51-53.
- Bottke, W.F., and Melosh, H.J., 1996b. Binary asteroids and the formation of doublet craters. *Icarus* 124, 372-391.
- Bottke, W.F., Vokrouhlicky, D., Rubincam, D.P., and Broz, M. 2002. The effect of Yarkovsky thermal forces on the dynamical evolution of asteroids and meteoroids. In: Bottke, W.F., Cellino, A., Paolicchi, P., and Binzel, R.P. (Eds.), *Asteroids III*. Univ. of Arizona Press, Tucson, pp. 395-408.

- Chauvineau, B., Farinella, P., and Harris, A.W., 1995. The evolution of Earth-approaching binary asteroids: A Monte Carlo dynamical model. *Icarus* 115, 36-46.
- Farinella, P. 1992. Evolution of Earth-crossing binary asteroids due to gravitational encounters with the Earth. *Icarus* 96, 284-285.
- Hudson, R.S., and Ostro, S.J., 1994. Shape of asteroid 4769 Castalia (1989 PB) from inversion of radar images. *Science* 263, 940-943.
- Hudson, R.S., and Ostro, S.J., 1995. Shape and non-principal axis spin state of asteroid 4179 Toutatis. *Science* 270, 84-86.
- Hudson, R.S., Ostro, S.J., Jurgens, R.F., Rosema, K.D., Giorgini, J.D., Winkler, R., Rose, R., Choate, D., Cormier, R.A., Franck, C.R., Frye, R., Howard, D., Kelley, D., Littlefair, R., Slade, M.A., Benner, L.A.M., Thomas, M.L., Mitchell, D.L., Chodas, P.W., Yeomans, D.K., Scheeres, D.J., Palmer, P., Zaitsev, A., Koyama, Y., Nakamura, A., Harris, A.W., and Meshkov, M.N., 2000. Radar observations and physical model of asteroid 6489 Golevka. *Icarus* 148, 37-51.
- Hudson, R.S., Ostro, S.J., and D. J. Scheeres, D.J., 2003. High-resolution model of asteroid 4179 Toutatis. *Icarus* 161, 346-355.
- Jurgens, R.F., and Goldstein, R.M., 1976. Radar observations at 3.5 and 12.6 cm wavelength of asteroid 433 Eros. *Icarus* 28, 1-15.
- Krugly, Y.N., Belskaya, I.N., Shevchenko, V.G., Chiorny, V.G., Velichko, F.P., Mottola, S., Erikson, A., Hahn, G., Nathues, A., Neukum, G., Gaftonyuk, N.M., and Dotto, E., 2002. The near-Earth objects follow-up program. IV. CCD photometry in 1996-1999. *Icarus* 158, 294-304.
- Leinhardt, Z.M., Richardson, D.C., and Quinn, T. 2000. Direct N-body simulations of rubble pile collisions. *Icarus* 146, 133-151.
- Magri, C., Consolmagno, G.J., Ostro, S.J., Benner, L.A.M., and Beeny, B.R., 2001. Radar constraints

on asteroid regolith compositions using 433 Eros as ground truth. *Meteorit. Planet. Sci.* 36, 1697-1709.

Margot, J.L., Nolan, M.C., Benner, L.A.M., Ostro, S.J., Jurgens, R.F., Giorgini, J.D., Slade, M.A., and Campbell D.B., 2002. Binary asteroids in the near-Earth object population. *Science* 296, 1445-1448.

Merline, W.J., Weidenschilling, S.J., Durda, D.D., Margot, J.L., Pravec, P., and Storrs, A.D., 2002. Asteroids *do* have satellites. In: Bottke, W.F., Cellino, A., Paolicchi, P., and Binzel, R.P., (Eds.), *Asteroids III*. Univ. of Arizona Press, Tucson, pp. 289-312.

Ostro, S.J., Campbell, D.B., and Shapiro, I.I., 1983. Radar observations of asteroid 1685 Toro. *Astron. J.* 88, 565-576.

Ostro, S.J., Chandler, J.F., Hine, A.A., Rosema, K.D., Shapiro, I.I., and Yeomans, D.K., 1990. Radar images of asteroid 1989 PB. *Science* 248, 1523-1528.

Ostro, S.J., Hudson, R.S., Jurgens, R.F., Rosema, K.D., Campbell, D.B., Yeomans, D.K., Chandler, J.F., Giorgini, J.D., Winkler, R., Rose, R., Howard, S.D., Slade, M.A., Perillat, P., and Shapiro, I.I., 1995. Radar images of asteroid 4179 Toutatis. *Science* 270, 80-83.

Ostro, S.J., Jurgens, R.F., Rosema, K.D., Hudson, R.S., Giorgini, J.D., Winkler, R., Yeomans, D.K., Choate, D., Rose, R., Slade, M.A., Howard, S.D., Scheeres, D.J., and Mitchell, D.L., 1996. Radar observations of asteroid 1620 Geographos. *Icarus* 121, 46-66.

Ostro, S.J., Hudson, R.S., Benner, L.A.M., Nolan, M.C., Margot, J.L., Giorgini, J.D., Jurgens, R.F., Rose, R., and Yeomans, D.K., 2000. Radar observations of asteroid 4486 Mithra. *Bull. Am. Astron. Soc.* 32, 1003.

Ostro, S.J., Hudson, R.S., Benner, L.A.M., Giorgini, J.D., Magri, C., Margot, J.L., and Nolan, M.C., 2002. Asteroid radar astronomy. In: Bottke, W.F., Cellino, A., Paolicchi, P., and Binzel, R.P.,

2003. (Eds.), Asteroids III. Univ. of Arizona Press, Tucson, pp. 151-168.
- Ostro, S.J., Benner, L.A.M., Nolan, M.C., Magri, C., Giorgini, J.D., Scheeres, D.J., Broschart, S.B., Kaasalainen, M., Vokrouhlicky, D., Chesley, S.R., Margot, J.L., Jurgens, R.F., Rose, R., Yeomans, D.K., Suzuki, S., and DeJong, E.M., 2004. Radar observations of asteroid 25143 Itokawa (1998 SF36). *Meteorit. Planet. Sci.* 39, 407-424.
- Ostro, S.J., Benner, L.A.M., Magri, C., Giorgini, J.D., Rose, R., Jurgens, R.F., Yeomans, D.K., Hine, A.A., Nolan, M.C., Scheeres, D.J., Kaasalainen, M., Vokrouhlicky, D., Chesley, S.R., and Margot, J.L., 2005. Radar observations of Itokawa in 2004 and an improved physical model. Submitted for publication.
- Pravec, P., Wolf, M., and Sarounova, S., 1998. Lightcurves for 26 near-Earth asteroids. *Icarus* 136, 124-136.
- Pravec, P., Harris, A.W., Scheirich, P., Kusnirak, P., Sarounova, L., Hergenrother, C.W., Mottola, S., Hicks, M.D., Masri, G., Krugly, Y.N., Shevchenko, V.G., Nolan, M.C., Howell, E.S., Kaasalainen, M., Galad, A., Brown, P., DeGraff, D.R., Lambert, J.V., Cooney, W.R., and Foglia, S., 2005. Tumbling asteroids. *Icarus* 173, 108-131.
- Pravec, P., Scheirich, P., Kusnirak, P., Sarounova, L., Mottola, S., Hahn, G., Brown, P., Esquerdo, G., Kaiser, N., Krzeminski, Z., Pray, D.P., Warner, B.D., Nolan, M.C., Howell, E.S., Benner, L.A.M., Harris, A.W., Galad, A., Holliday, W., Hicks, M.D., Krugly, Y.N., Tholen, D., Whiteley, R., Marchis, F., DeGraff, D.R., Grauer, A., Larson, S., Velichko, F.P., Cooney, W.R., Stephens, R., Zhu, J., Kirsch, K., Dyvig, R., Snyder, L., Reddy, V., Moore, S., Gajdos, S., Vilagi, J., Masi, G., Higgins, D., Funkhouser, G., Knight, B., Slivan, S., Behrend, R., Roy, R., Demeautis, C., Matter, D., Waelchli, N., Revaz, Y., Klotz, A., Rieugne, M., Thierry, P., Cotrez, V., Brunetto, L., Kober, G., 2005. Photometric survey of binary near-Earth asteroids. Submitted

for publication.

Richardson, D.C., Bottke, W.F., and Love, S.G., 1998. Tidal distortion and disruption of Earth-crossing asteroids. *Icarus* 134, 47-76.

Scheeres, D.J., Marzari, F., and Rossi, A., 2004. Evolution of NEO rotation rates due to close encounters with Earth and Venus. *Icarus* 170, 312-323.

Taylor, P.A., Margot, J.L., Nicholson, P.D., Campbell, D.B., Jurgens, R.F., Ostro, S.J., Benner, L.A.M., Giorgini, J.D., Nolan, M.C., Howell, E.S., Hine, A.A., and Hudson, R.S., 2004. Properties of horseshoe object 2000 PH5 from radar observations. *Bull. Am. Astron. Soc.* 36, 1181.

[Abstract]

TABLES

TABLE 1: Observations

setup	code	OSOD	Runs	start	stop
CW		14	5	040341	041425
CW		16	1	041800	041904
4.0 μ s	8191	16	2	042742	043110
4.0 μ s	1023	16	1	043411	043515
0.1 μ s	65535	16	38	044301	061847

"Code" refers to the code length for the repetitive binary-phase-coded transmission. OSOD refers to the orbit solution computed using the JPL On-Site Orbit Determination software. Runs indicate the number of transmit-receive cycles with each setup. Start and stop refer to the UTC epochs at the beginning and end of reception of echoes.

TABLE 2: Close Approaches

Date	Body	Close approach distance			Vrel (km s ⁻¹)	TCA3Sg (min)
		Nominal (AU)	Minimum (AU)	Maximum (AU)		
1784 Feb 24.51637	Earth	0.0740	0.0689	0.1210	16.45	5339.4
1834 Feb 26.04347	Earth	0.0687	0.0685	0.0709	16.25	1037.3
1884 Feb 26.28460	Earth	0.0675	0.0672	0.0680	16.30	221.73
1934 Feb 24.45098	Earth	0.0851	0.0836	0.0867	16.84	168.12
2005 Feb 26.78912	Earth	0.0628	0.0628	0.0628	16.25	0.03
2076 Feb 25.30201	Earth	0.0742	0.0728	0.0756	16.75	175.28
2168 Feb 26.56088	Earth	0.0692	0.0681	0.0703	16.65	158.71
2260 Feb 28.77030	Earth	0.0586	0.0586	0.0586	16.33	1.15
2276 Aug 26.01322	Vesta	0.0677	0.0672	0.0682	11.81	7.44
2352 Mar 05.62944	Earth	0.0994	0.0979	0.1009	15.35	146.46
2352 Nov 14.27346	Vesta	0.0362	0.0355	0.0369	12.30	40.07
2423 Mar 04.81225	Earth	0.0786	0.0774	0.0799	15.56	150.60
2494 Mar 05.81649	Earth	0.0955	0.0931	0.0979	15.32	242.00
2565 Mar 06.54070	Earth	0.0957	0.0934	0.0980	15.28	239.77
2610 Jul 23.65853	Vesta	0.0729	0.0722	0.0737	12.57	82.59
2686 Feb 26.91161	Earth	0.0902	0.0875	0.0930	17.31	253.00
2757 Feb 28.38674	Earth	0.0780	0.0778	0.0782	17.05	23.25
2991 Mar 08.92480	Earth	0.0916	0.0915	0.0918	15.08	12.84
3062 Mar 06.74220	Earth	0.0598	0.0580	0.0618	15.66	321.35
3133 Mar 07.85981	Earth	0.0652	0.0583	0.0735	15.51	1073.3
3183 Mar 02.74335	Earth	0.0775	0.0623	0.0954	17.10	1766.3
3254 Mar 05.33103	Earth	0.0530	0.0530	0.0540	16.14	684.04
3375 Mar 10.31777	Earth	0.0863	0.0860	0.0865	15.04	32.03
3454 Mar 04.28158	Earth	0.0716	0.0544	0.1407	16.91	6775.6
3504 Mar 04.71908	Earth	0.0720	0.0556	0.1508	16.90	7676.0
3575 Mar 10.80554	Earth	0.0787	0.0561	0.1263	15.14	5084.6
3625 Mar 06.09990	Earth	0.0588	0.0571	0.0638	16.34	1174.4

2005 CR37 close approaches using JPL orbit solution #30. This list of planetary encounters < 0.1 AU terminates at the last Earth encounter prior to the linearized 3σ time of close approach uncertainty (TCA3Sg) exceeding ± 10 days. CA Dist is the highest probability approach distance of the reference trajectory to the given body. MinDist and MaxDist are the 3σ distances from the body at the nominal encounter time. Vrel is the nominal relative velocity. Integrations were performed using the DE403 planetary ephemeris and include relativistic perturbations due to the Sun, planets, and Moon, and asteroids Ceres, Pallas, and Vesta.

TABLE 3: Radar properties

Run	$\sigma_{\text{OC}} \pm 25\%$ (km ²)	SC/OC
1	0.14	0.33 \pm 0.01
2	0.15	0.28 \pm 0.01
3	0.16	0.31 \pm 0.01
4	0.17	0.31 \pm 0.01
5	0.17	0.37 \pm 0.01
6	0.19	0.30 \pm 0.01
Mean	0.16	0.32 \pm 0.03

σ_{OC} is the OC radar cross section; uncertainties are dominated by systematic pointing and calibration errors. The cross sections and SC/OC were estimated using a frequency resolution of 0.5 Hz in order to have enough fast-Fourier Transforms ($N = 60$) to produce nearly Gaussian noise statistics. For SC/OC, systematic effects cancel and most remaining statistical errors propagate from receiver thermal noise. The last row lists the mean for σ_{OC} and the mean and rms dispersion for SC/OC.

TABLE 4: Candidate Contact Binary NEAs

Asteroid	Diameter (km)	Res'n (m)	Rotation period (h)	Shape Reference
68346 2001 KZ66	1.0	15	2.7	Nolan et al., unpublished
4769 Castalia	1.0	300	4 ^a	Ostro et al. 1990, Hudson and Ostro 1994
2005 CR37	1.0	15	5.6 ^b	This paper
11066 Sigurd	3.0	75	8.5 ^{cd}	Benner et al. 2004
2063 Bacchus	0.6	75	15.1 ^c	Benner et al. 1999
2002 NY40	0.4	15	20 ^e	NPA Pravec et al. 2005
4486 Mithra	2.4	19	~100 ^e	NPA Ostro et al. 2000
2002 FC	0.7	15	days	Ostro et al., unpublished
52387 1993 OM7	1.0	15	weeks	Ostro et al., unpublished
2004 RF84	2.4	15	weeks	Benner et al. unpublished

Candidate contact binary NEAs imaged by delay-Doppler radar observations. “Res’n” indicates the range resolution of delay-Doppler radar images. "NPA" indicates non-principal axis rotation. The objects are listed in order of increasing rotation period. Rotation periods are from the references indicated. Rotation periods without references were estimated from sequences of unpublished radar images.

^aOstro et al. 1990.

^bD. Pray, pers. comm.

^cPravec et al. 1998

^dKrugly et al. 2002

^ePravec et al. 2005

FIGURE CAPTIONS

FIGURE 1:

2005 CR37 radar movie. Our 1.6-hour sequence of 38 runs is arranged chronologically, from left to right and top to bottom. Images are 64-s integrations separated by 80 s. Range increases from top to bottom and Doppler frequency increases from left to right, so rotation is counterclockwise. The resolution is $0.1 \mu\text{s}$ (15 m) \times 0.07 Hz (\sim 14 m horizontally for an equatorial view). The images have the same logarithmic contrast stretch in order to take advantage of the dynamic range.

FIGURE 2

Enlarged images of three runs from the beginning, middle, and end of the track. Delay-Doppler extents and orientations are the same as in Fig. 1. Arrows indicate features described in the text. Times spanned by each image are given at the bottom. The images have the same logarithmic contrast stretch in order to take advantage of the dynamic range.

FIGURE 3

Echo power spectra from each run, shown at 0.5-Hz resolution, arranged chronologically from top to bottom.

Fig. 1

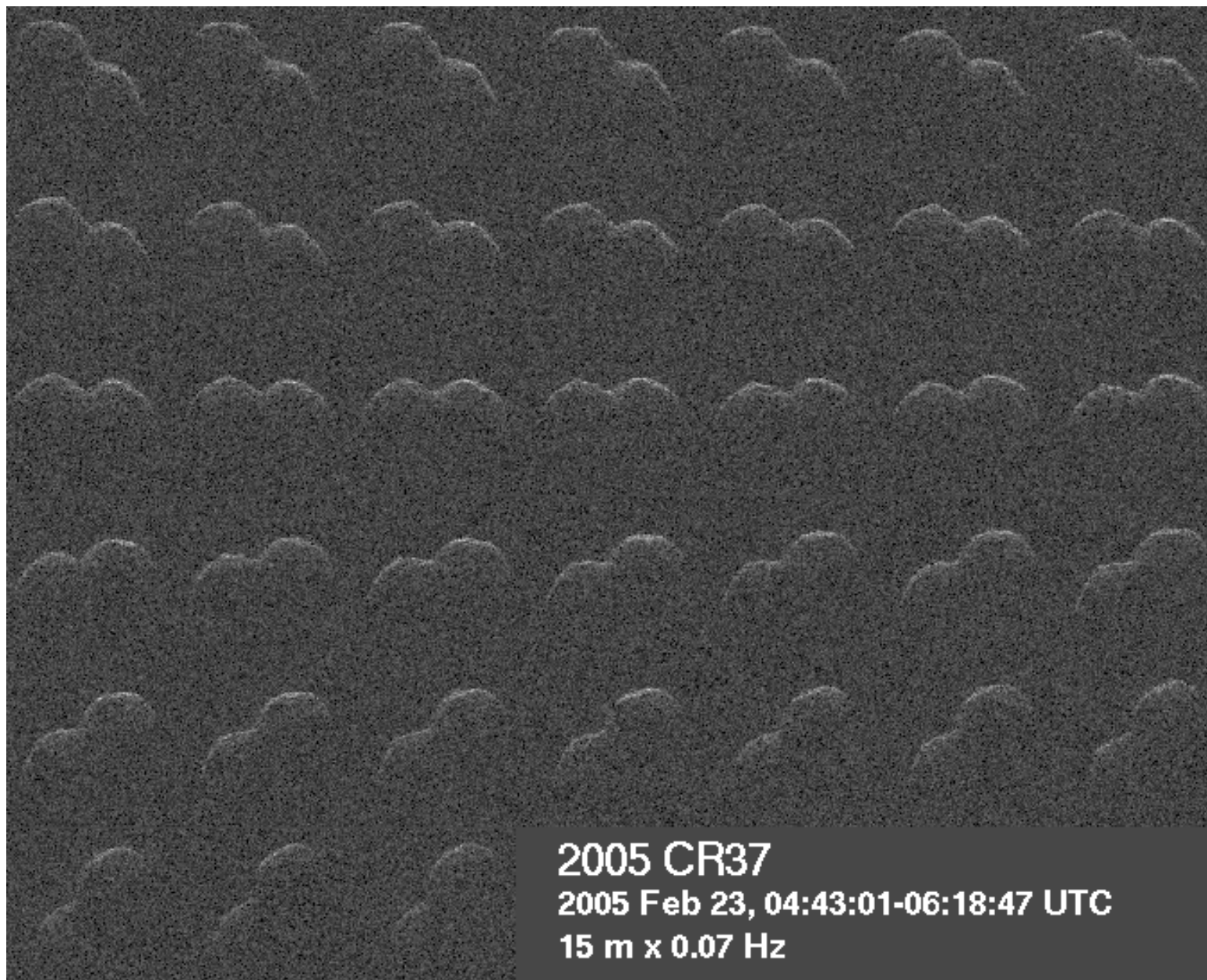
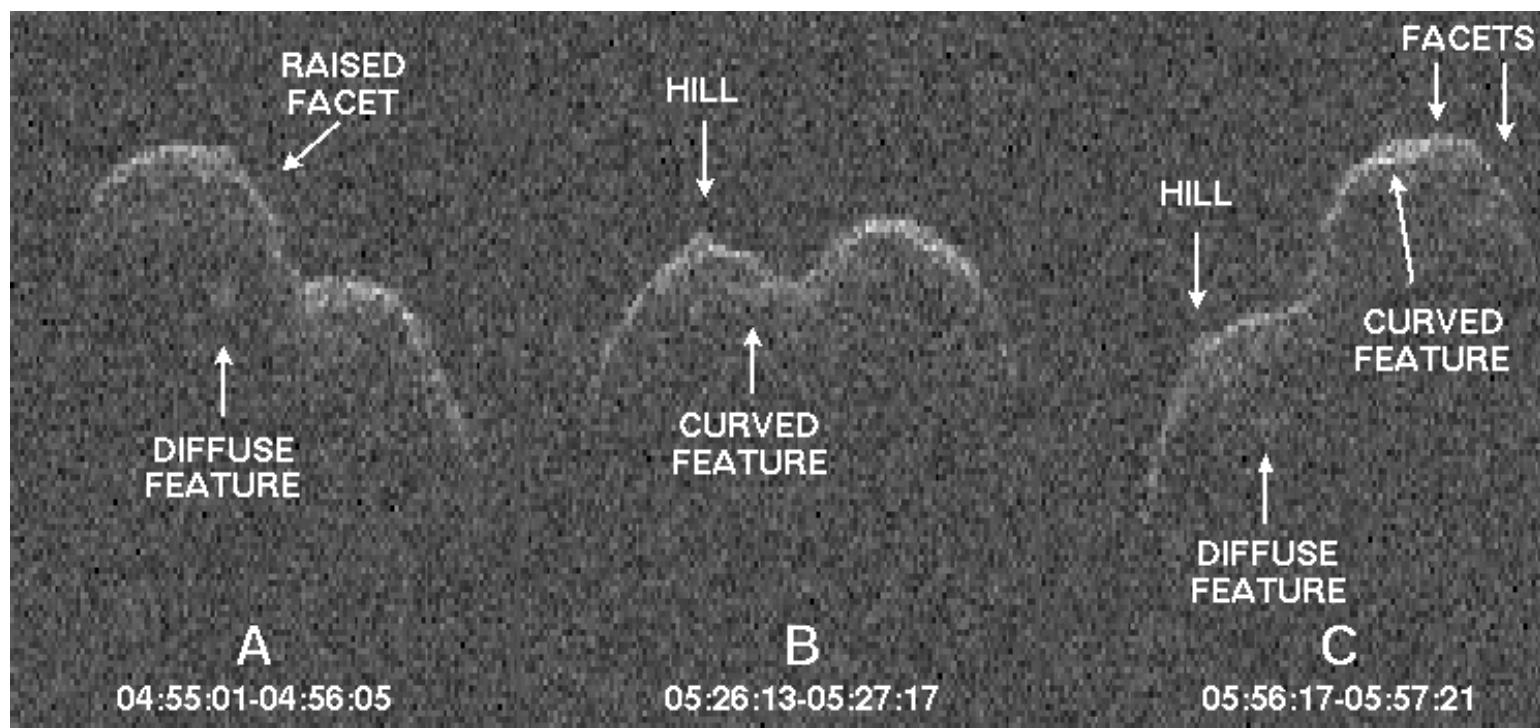


Fig. 2



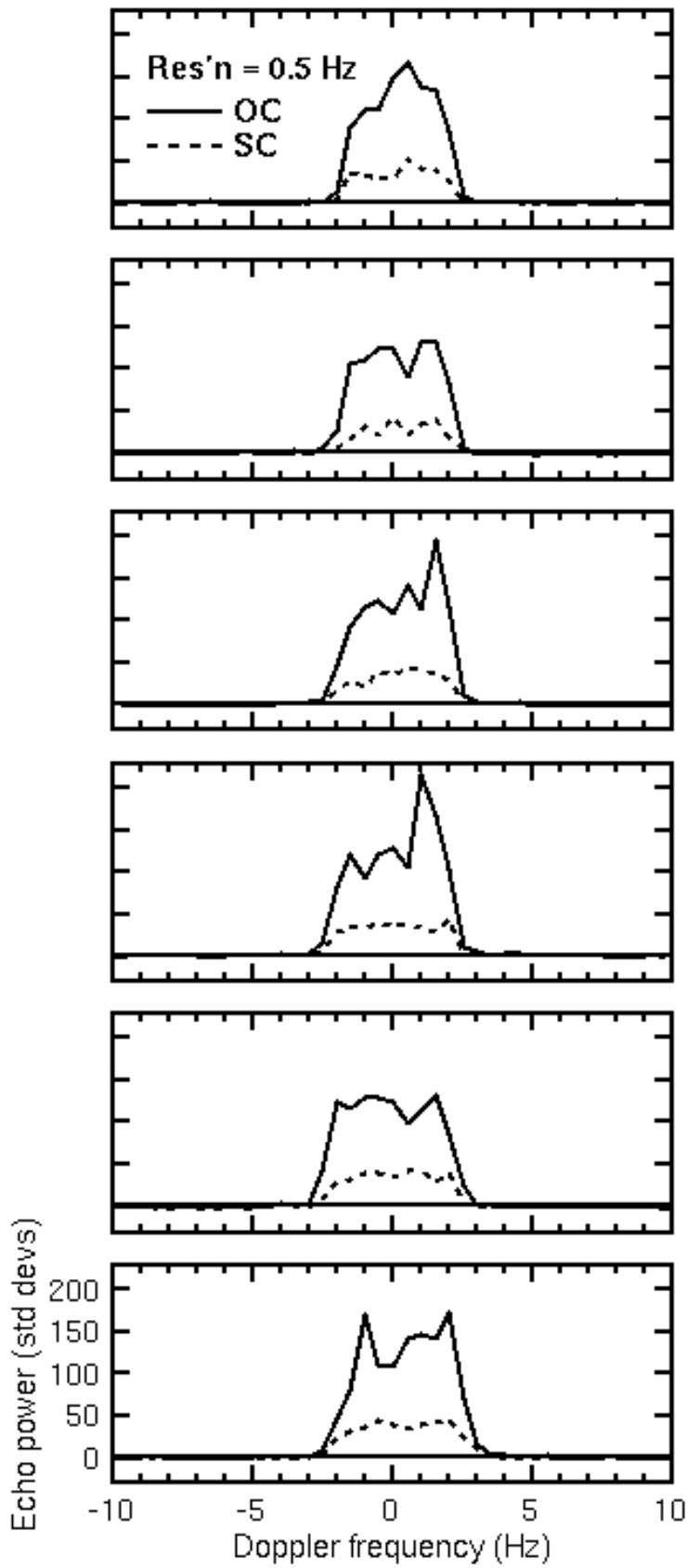


Fig. 3